arXiv:1409.4537v1 [physics.flu-dyn] 16 Sep 2014

Homogeneous Isotropic Superfluid Turbulence in Two Dimensions: Inverse and Forward Cascades in the Hall-Vinen-Bekharevich-Khalatnikov model

Vishwanath Shukla,[1,*] Anupam Gupta,[2,†] and Rahul Pandit[3,‡]

[1] *Centre for Condensed Matter Theory, Department of Physics, Indian Institute of Science, Bangalore 560012, India*
[2] *Department of Physics, University of Rome Tor Vergata, Via della Ricerca Scientifica 1, 00133 Rome, Italy*
[3] *Centre for Condensed Matter Theory, Department of Physics, Indian Institute of Science, Bangalore 560012, India.*

(Dated: September 17, 2014)

We present the first direct-numerical-simulation study of the statistical properties of two-dimensional superfluid turbulence in the Hall-Vinen-Bekharevich-Khalatnikov two-fluid model. We show that both normal-fluid and superfluid energy spectra can exhibit two power-law regimes, the first associated with an inverse cascade of energy and the second with the forward cascade of enstrophy. We quantify the mutual-friction-induced alignment of normal and superfluid velocities by obtaining probability distribution functions of the angle between them and the ratio of their moduli. Our study leads to specific suggestions for experiments.

PACS numbers: 47.27.Gs, 47.27.ek, 47.37.+q, 67.25.dm
Keywords: superfluid; turbulence; two-fluid model

The elucidation of superfluid turbulence, a problem of central importance in quantum fluids and nonequilibrium statistical mechanics, continues to provide challenges for experiments, theory, and numerical simulations [1–4]. Such turbulence has been studied more often in three dimensions (3D) than in two dimensions (2D). It is well known that 2D and 3D *fluid* turbulence are qualitatively different [5–8]; similar differences have not been explored in detail for *superfluid* turbulence. Therefore, we initiate a study of the statistical properties of 2D homogeneous, isotropic, superfluid turbulence, at the level the Hall-Vinen-Bekharevich-Khalatnikov (HVBK), two-fluid model [4, 9–12], with the specific goal of elucidating the natures of both inverse and forward cascades of energy and enstropy, the mean square vorticity. Homogeneous, isotropic, 2D and 3D fluid turbulence are essentially different because, in the former, both the energy and the enstrophy are conserved in the inviscid, unforced limit, whereas, in the latter, only the energy is conserved [5–8]. Therefore, in 2D fluid turbulence, energy, injected at a wave number $k_{\rm f}$, shows an inverse cascade towards large length scales (wave number $k < k_{\rm f}$), whereas the enstrophy displays a forward cascade to small length scales ($k > k_{\rm f}$); these inverse and forward cascades yield, respectively, energy spectra that scale as $E(k) \sim k^{-5/3}$ and $E(k) \sim k^{-\delta}$, where δ depends on the friction ($\delta = 3$ if there is no friction). By contrast, 3D fluid turbulence shows only a forward cascade of energy with $E(k) \sim k^{-5/3}$, at the level of Kolmogorov's (K41) phenomenological theory [5] and for $k_f \ll k \ll k_d$, where k_d is the wave number scale at which viscous dissipation becomes significant.

Our direct numerical simulation (DNS), which we have designed to study the statistical properties of inverse and forward cascades in the HVBK model, yields several interesting results that have not been anticipated hitherto: (1) Both normal-fluid and superfluid energy spectra, $E^n(k)$ and $E^s(k)$, respectively, show inverse- and forward-cascade power-law regimes. (2) The forward-cascade power law depends on (a) the friction coefficient, as in 2D fluid turbulence, and, in addition, on (b) the coefficient B of mutual friction, which couples normal and superfluid velocities. (3) As B increases, the normal and superfluid velocities, $\mathbf{u}_n$ and $\mathbf{u}_s$, respectively, tend to get locked to each other, and, therefore, $E^s(k) \simeq E^n(k)$, especially in the inverse-cascade regime. (4) We quantify this locking tendency by calculating the probability distribution functions (PDFs) $P(\cos(\theta))$ and $P(\gamma)$, where the angle $\theta \equiv \cos^{-1}((\mathbf{u}_{\rm n} \cdot \mathbf{u}_{\rm s})/(|\mathbf{u}_{\rm n}||\mathbf{u}_{\rm s}|))$ and the amplitude ratio $\gamma = |\mathbf{u}_{\rm n}|/|\mathbf{u}_{\rm s}|$; the former has a peak at $\cos(\theta) = 1$; and the latter exhibits a peak at $\gamma = 1$ and power-law tails on both sides of this peak. (5) This locking increases as we increase B, but the power-law exponents for the tails of $P(\gamma)$ are universal, in so far as they do not depend on B, ρ_n/ρ, where ρ_n and ρ are normal-fluid and total densities, respectively, and $k_{\rm f}$.

The incompressible, 2D HVBK equations are [4, 9–12]

$$D_t \mathbf{u}_{\rm n} = -\frac{1}{\rho_{\rm n}}\nabla p_{\rm n} + \nu_{\rm n}\nabla^2 \mathbf{u}_{\rm n} - \mu_{\rm n}\mathbf{u}_{\rm n} + \mathbf{F}^{\rm n}_{\rm mf} + \mathbf{f}^{\rm n}_u, \quad \text{(1a)}$$

$$D_t \mathbf{u}_{\rm s} = -\frac{1}{\rho_{\rm s}}\nabla p_{\rm s} + \nu_{\rm s}\nabla^2 \mathbf{u}_{\rm s} - \mu_{\rm s}\mathbf{u}_{\rm s} + \mathbf{F}^{\rm s}_{\rm mf} + \mathbf{f}^{\rm s}_u, \quad \text{(1b)}$$

where $D_t \mathbf{u}_i \equiv \partial_t + \mathbf{u}_i \cdot \nabla$, $\nabla \cdot \mathbf{u}_i = 0$ is the incompressibility condition, and the subscript $i \in ({\rm n}, {\rm s})$ denotes the normal fluid (n) or the superfluid (s); ρ_i, p_i, and ν_i are the density, partial pressure, and viscosity, respectively, of the component i. Linear-friction terms, with coefficients μ_i, model air-drag-induced or bottom friction. For the

superfluid $\nu_{\rm s}$ and $\mu_{\rm s}$ are zero, but any DNS study must use $\nu_{\rm s}(\neq 0) \ll \nu_{\rm n}$ and $\mu_{\rm s} \ll \mu_{\rm n}$ to avoid numerical instabilities and to achieve a statistically steady state. The mutual-friction terms can be written as $\mathbf{F}^{\rm n}_{\rm mf} = (\rho_s/\rho)\mathbf{f}_{\rm mf}$ and $\mathbf{F}^{\rm s}_{\rm mf} = -(\rho_n/\rho)\mathbf{f}_{\rm mf}$ in Eqs. (1a) and (1b), respectively, where

$$\mathbf{f}_{\rm mf} = \frac{B}{2}\frac{\omega_{\rm s}}{|\omega_{\rm s}|} \times (\omega_{\rm s} \times \mathbf{u}_{\rm ns}) + \frac{B'}{2}\omega_{\rm s} \times \mathbf{u}_{\rm ns}, \qquad (2)$$

with $\mathbf{u}_{\rm ns} = (\mathbf{u}_{\rm n} - \mathbf{u}_{\rm s})$ the slip velocity, and B and B' the coefficients of mutual friction. In most of our studies we set $B' = 0$ so, in 2D, $\mathbf{f}_{\rm mf} = -\frac{B}{2}|\omega_{\rm s}|\mathbf{u}_{\rm ns}$. (We have checked in one representative case that our results do not change qualitatively if $B' > 0$.) In our DNS, we use the stream-function ψ_i and vorticity $\omega_i = \nabla \times \mathbf{u}_i = -\nabla^2\psi_i$ formulation [13]. To obtain a statistically steady state, we force the vorticity field with a Kolmogorov-type term $f^i_\omega = -f^i_0 k^i_{\rm f} \cos(k^i_{\rm f} x)$, where f^i_0 and $k^i_{\rm f}$ are the amplitude and the forcing wave number, respectively. We use (a) $k^i_{\rm f} = 2$ and (b) $k^i_{\rm f} = 50$; the former leads to energy spectra that are dominated by a forward cascade of enstrophy, whereas the latter yields spectra with an inverse cascade of energy and a forward cascade of enstrophy; we force the dominant component in case (b) (i.e., the normal-fluid (superfluid) component if $\rho_n/\rho > 0.5$ ($\rho_n/\rho \leq 0.5$)).

We perform a DNS of Eqs. (1a) and (1b) with periodic boundary conditions, on a square simulation domain with side $L = 2\pi$, by using a pseudospectral method [13, 14] with N_c^2 collocation points and the 2/3 dealiasing rule. For time evolution we use a second-order, exponential time differencing Runge-Kutta method [15]. The parameters of our DNS runs are given in Table I (and in the Supplemental Material [16]). We characterize our system by computing the spectra $E_n(k)$ and $E_s(k)$, $E_i(k) = \langle \sum_{k-\frac{1}{2}<k'\leq k+\frac{1}{2}} |\mathbf{u}_{\rm i}(\mathbf{k}', t)|^2 \rangle_t$ ($\langle\rangle_t$ denotes a time average), the probability distribution functions (PDFs) $P(\omega_i)$ of the vorticities and $P(\cos(\theta))$, the cumulative PDF $Q(\gamma)$ of γ, energy and enstrophy fluxes $\Pi_{\rm i}(k,t)$ and $Z_{\rm i}(k)$ ($i \in$ (n, s)), respectively, and the mutual-friction transfer function $M_{\rm i}(k)$, which we define below.

In Fig. 1 we present pseudocolor plots of ω_n and ω_s for run `R1` (panels (a) and (b)). Similar plots for run `R2a` with $k_{\rm f} = 50$ are given in Fig. 1 in the Supplemental Material [16]. The sizes of the vortical regions in these plots are $\sim k_{\rm f}^{-1}$ (as in 2D fluid turbulence with friction [7, 13]). Figures 1 (a) and (b) show that the normal and superfluid components are nearly locked to each other; this is illustrated dramatically in Video M1 [16], in which the lower two panels show the spatiotemporal evolution of Figs. 1 (a) and (b) and the top two panels show how ω_n and ω_s evolve in the absence of mutual friction (i.e., $B = B' = 0$); in the latter case, ω_n evolves to a frozen, stationary state; however, if $B > 0$, then the turbulence in the superfluid component is transferred to the normal component (top two panels of Video M1). Such a transfer of turbulence has been envisaged in 3D superfluid turbulence [17–19] but never displayed as graphically as in our Video M1.

We quantify the locking of the normal and superfluid velocities by plotting, in Fig. 1 (c), for the illustrative runs `R1` and `R2a`-`R2c`, the PDF $P(\cos(\theta))$, which shows

	ρ_n/ρ	B	ν_n	ν_s	$k^{\rm n}_f$	$k^{\rm s}_f$	$f^{\rm n}_0$	$f^{\rm s}_0$	Re^n_λ	Re^s_λ
`R0`	–	–	10^{-4}	10^{-5}	2	2	10^{-3}	10^{-3}	92.77	1.25×10^3
`R1`	0.1	1.0	10^{-4}	10^{-5}	2	2	10^{-3}	10^{-3}	112.9	1.3×10^3
`R2a`	0.1	1.0	10^{-4}	10^{-5}	–	50	–	10^{-1}	108.4	876.7
`R2b`	0.1	2.0	10^{-4}	10^{-5}	–	50	–	10^{-1}	100.6	876.8
`R2c`	0.1	5.0	10^{-4}	10^{-5}	–	50	–	10^{-1}	94.3	876.5
`R3`	0.05	1.0	10^{-4}	10^{-5}	–	50	–	10^{-1}	119.1	976.7
`R4`	0.3	1.0	10^{-4}	10^{-5}	–	50	–	10^{-1}	62.9	487.6
`R5`	0.5	1.0	10^{-5}	10^{-6}	–	50	–	10^{-1}	484.1	4.1×10^3
`R6`	0.9	1.0	10^{-5}	10^{-6}	50	–	10^{-1}	–	617.0	7.19×10^3

TABLE I. Parameters for our DNS runs `R0`-`R6` with $N_c^2 = 1024^2$ collocation points: ρ_n/ρ is the fraction of the normal fluid, B the mutual-friction coefficient, ν_n (ν_s) the normal-fluid (superfluid) kinematic viscosity, and $k^n_{\rm f}$ ($k^s_{\rm f}$) and f^n_0 (f^s_0) are the forcing wave vector and the forcing amplitude for the normal fluid (superfluid). The coefficient of linear friction for the normal fluid (superfluid) $\mu_n = 10^{-2}$ ($\mu_s = 5 \times 10^{-3}$) is kept fixed. For more parameters see Table 1 in [16].

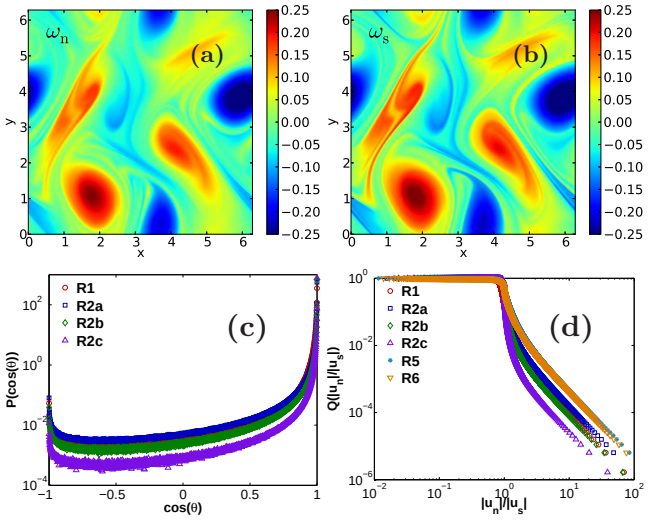

FIG. 1. (Color online) Pseudocolor plots of the vorticity fields, ω_n and ω_s, from our DNS run `R1` at $t = 1720$ (panels (a) and (b), $k_{\rm f} = 2$); these plots show that the normal and superfluid component are locked to each other. (c) Semilogarithmic (base 10) plots of the PDF $P(\cos(\theta))$ of the angle θ between $\mathbf{u}_{\rm n}$ and $\mathbf{u}_{\rm s}$ for runs `R1` (red circles), `R2a` ($B = 1$, blue squares), `R2b` ($B = 2$, green diamonds), and `R2c` ($B = 5$, purple triangles). (d) Log-log (base 10) plots of the complementary cumulative distribution functions (CDF) $R(\gamma)$ of $\gamma = |\mathbf{u}_{\rm n}|/|\mathbf{u}_{\rm s}|$ for the runs `R1`, `R2a` – `R2c`, `R5`, and `R6`. These CDFs show power-law tails ($R(\gamma) \sim \gamma^{-2}$) that imply $P(\gamma) \sim \gamma^{-3}$, for $\gamma \gg 1$.

a peak at $\cos(\theta) = 1$ and falls rapidly with increasing θ; this indicates that $\mathbf{u}_{\rm n}(\mathbf{r},t)$ and $\mathbf{u}_{\rm s}(\mathbf{r},t)$ align preferentially along the same direction; the degree of alignment increases as we increase B. In Figs. 1 (d) we show, respectively, plots of the complementary cumulative distribution functions (CDFs) $R(\gamma)$ of $\gamma = |\mathbf{u}_{\rm n}|/|\mathbf{u}_{\rm s}|$, for the runs `R1`, `R2a-R2c`, `R5`, and `R6`. These CDFs exhibit power-law tails that imply that $P(\gamma) \sim \gamma^{-3}$, for $\gamma \gg 1$ (A similar analysis of the left tail [16] yields $P(\gamma) \sim \gamma$, for $\gamma \ll 1$). The power-law exponents of these tails of $P(\gamma)$ are universal in the sense that they do not depend on B, $\rho_{\rm n}/\rho$, and $k_{\rm f}$.

Figure 2 (a) compares energy spectra from runs `R0` and `R1`, in which there are no inverse-cascade regimes in energy spectra; this figure illustrates how the mutual-friction-induced interaction between the two components modifies the energy spectra $E_i(k,t)$. For the run `R0`, in which $B = 0$ and, therefore, the normal and superfluid components are uncoupled, $E^n(k)$ and $E^s(k)$ are shown in Fig. 2 (a) by full and dashed purple lines, respectively: the power-law regimes, more prominent in $E^s(k)$ than in $E^n(k)$, are characterized by different, apparent scaling exponents, because the normal-fluid Reynolds number is too small for fully developed, normal-fluid turbulence. When we couple the normal and superfluid components, as in the run `R1`, $E^n(k)$ (green full curve in Fig. 2 (a)) is pulled up towards $E^s(k)$ (green dashed curve in Fig. 2 (a)), by virtue of the locking tendency that we have mentioned above; furthermore, both $E^n(k)$ and $E^s(k)$ now (i) display $k^{-\delta}$ forward-cascade, scaling ranges, with $\delta \simeq 4.2$, (ii) lie very close to each other at small wave numbers, and (iii) show dissipation regions at much higher wave numbers than in their counterparts when there is no coupling ($B = 0$ and run `R0`).

To study dual cascades, i.e., (i) an inverse cascade of energy for $k < k_{\rm f}$ and (ii) a direct cascade of enstrophy for $k > k_{\rm f}$, we use our DNS runs `R2a-R6` (see Table I). Figure 2 (b) shows $E^n(k)$ (full curves) and $E^s(k)$ (dashed curves) with dual cascades, for the runs `R2a` with $B = 1$ (purple curves), `R2b` with $B = 2$ (green curves), and `R2c` with $B = 5$ (blue curves). The inverse-cascade inertial ranges (with $k < k_{\rm f}$) of $E^n(k)$ and $E^s(k)$ exhibit scaling that is consistent with a $k^{-5/3}$ form (orange, dashed line), whereas the forward-cascade ranges (with $k > k_{\rm f}$) are consistent with $k^{-\delta}$ scaling, and $\delta \simeq 4.2$ (black, dashed line). In the forward-cascade regime of 2D fluid turbulence, the value of δ depends on the coefficient of linear friction [7, 13, 20, 21]; we find that, in the 2D HVBK model, δ depends not only on the coefficients of linear friction, but also on B. Furthermore, the locking that we have discussed above makes $E^n(k)$ and $E^s(k)$ lie more-or-less on top of each other for a considerable range of wave numbers; not surprisingly, this range of overlap increases as B increases; for $B = 5$ it extends into the direct-cascade region. Figure 2 (c) shows inverse- and forward-cascade regimes in log-log plots of $E^n(k)$ (full curves) and $E^s(k)$ (dashed curves) versus k for five representative values of $\rho_{\rm n}/\rho$ (runs R2a (purple curves), R3 (green curves), R4 (blue curves), R5 (black curves), and R6 (yellow curves)), with $B = 1$ and $k < k_{\rm f} = 50$.

The HVBK model allows us to study the evolution of two-fluid turbulence as we change $\rho_{\rm n}/\rho$, which is small at low temperatures and increases as the temperature increases and approaches the superfluid transition temperature; if $\rho_{\rm n}/\rho = 0.05$, HVBK turbulence is close to that of a pure superfluid, on the length and Mach-number scales at which the HVBK model is valid; in contrast, HVBK turbulence at $\rho_{\rm n}/\rho = 0.9$ is close to that of a classical, incompressible fluid. In Fig. 2 (c), the orange, dot-dashed line indicates a $k^{-5/3}$ power-law form that is visually close to the slopes (in log-log plots) of the energy spectra in the inverse-cascade scaling ranges; the black, dot-dashed line indicates a $k^{-4.2}$ power-law form that is visually close to the slope of the $E^n(k)$ spectrum in the forward-cascade scaling range for $\rho_{\rm n}/\rho = 0.9$. A complete study of the dependence of δ on $\mu_{\rm i}$ and B requires extensive, and high-resolution DNS studies whose current computational cost is prohibitive.

To characterize fluxes in the inverse- and forward-cascade regimes we use the energy-transfer relations for 2D, homogeneous, isotropic, HVBK, turbulence, namely,

$$\partial_{\rm t} E_{\rm i}(k,t) = -\mathcal{D}_{\rm i}(k,t) + \mathcal{T}_{\rm i}(k,t) + \mathcal{M}_{\rm i}(k,t) + \mathcal{F}^{\rm i}_o(k), \quad (3)$$

where $i \in (n,s)$, $\mathcal{D}_{\rm i}(k,t) \equiv \sum_{k-\frac{1}{2}<k'\le k+\frac{1}{2}} (\nu_{\rm i} k'^2 + \mu_{\rm i})|\mathbf{u}_{\rm i}(\mathbf{k}')|^2$ is the transfer function, which combines the effects of viscous dissipation and the friction, $\mathcal{T}_{\rm i}(k,t)$ is the kinetic-energy transfer because of the triad interactions of the Fourier components of the velocities, and $\mathcal{F}^{\rm i}_o(k)$ is the energy-injection spectrum for the component $i \in (n,s)$. The mutual-friction-induced exchange of energy between the normal and the superfluid components is measured by

$$\mathcal{M}_{\rm i}(k,t) \equiv \sum_{k-\frac{1}{2}<k'\le k+\frac{1}{2}} \mathbf{F}^{\rm i}_{\rm mf}(\mathbf{k}',t) \cdot \mathbf{u}_{\rm i}(-\mathbf{k}',t). \quad (4)$$

The kinetic-energy fluxes, through the wave number k, are $\Pi_{\rm i}(k,t) = \langle \int_k^{\rm k_{max}} \mathcal{T}_{\rm i}(k',t) dk' \rangle_t$; and their analogs for the enstrophy fluxes are $Z_{\rm i}(k)$ ($i \in (n,s)$). We plot these versus k in Figs. 2 (d) and (e), respectively, for the same runs (`R2a` and `R3-R6`) and the same color codes as in Fig. 2 (c). In Fig. 2 (d), for each one of these runs, the energy fluxes $\Pi_{\rm i}(k) < 0$, for $k < k_{\rm f}$, which confirms that we have inverse cascades of energy; in contrast, the enstrophy fluxes $Z_{\rm i}(k) > 0$, for $k > k_{\rm f}$, in Fig. 2 (e), so we have forward cascades of enstrophy. For the runs `R2a` and `R3-R6` we plot, in Fig. 2 (f), the transfer functions $M_i(k) = \langle \mathcal{M}_{\rm i}(k,t) \rangle_t$ versus k, which characterizes the energy exchange between the normal and superfluid components.

Other PDFs, e.g., those of velocity components and the vorticity, in 2D HVBK turbulence are qualita-

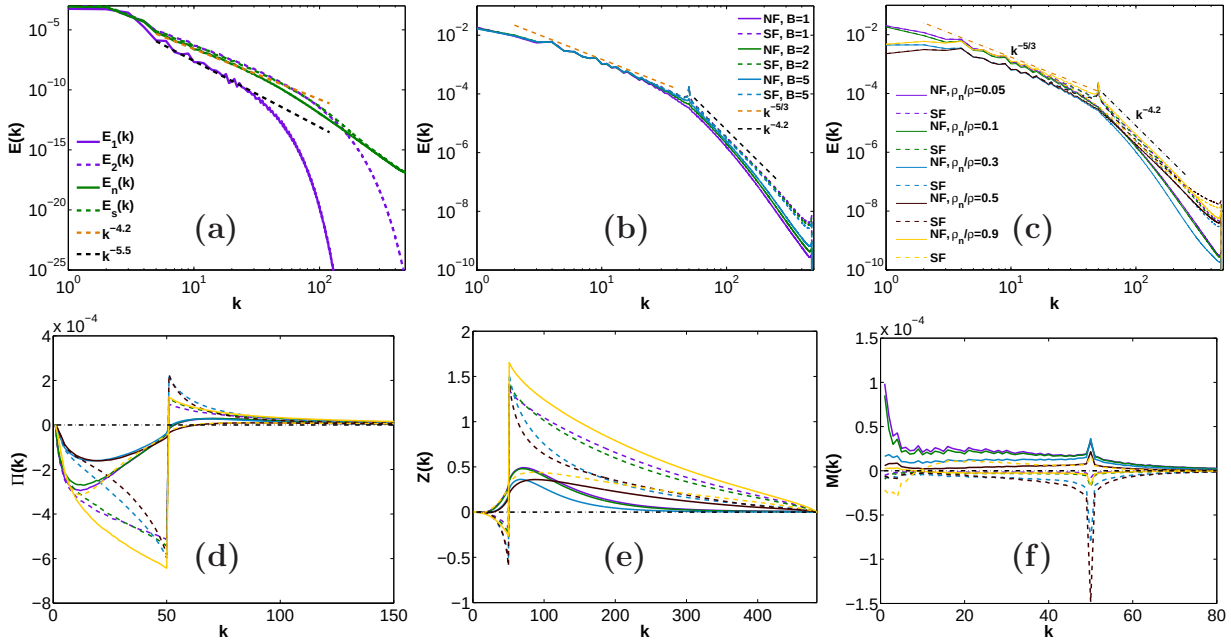

FIG. 2. (Color online) [Top panels] Log-log plots of the energy spectra $E_n(k)$ (full lines) and $E_s(k)$ (dashed lines) from our DNS runs: (a) `R0` ($B = 0$, purple lines) and `R1` ($B = 1$, green lines) with $k_f = 2$; (b) `R2a` ($B = 1$, purple curves), `R2b` ($B = 2$, green curves), and `R2c` ($B = 5$, sky-blue curves) with $k_f^s = 50$ and $\rho_n/\rho = 0.1$; (c) `R2a` (purple curves), `R3` (green curves), `R4` (sky-blue curves), `R5` (black curves), and `R6` (yellow curves), with $B = 1$; we force the dominant component. [Lower panels] Plots of (d) the energy flux $\Pi_i(k)$, (e) the enstrophy flux $Z_i(k)$, and (f) the mutual-friction transfer function $M_i(k)$, for the DNS runs represented in (c), with the same color codes as mentioned above. The abbreviation NF (SF) stands for normal-fluid (superfluid).

tively similar to their classical-fluid-turbulence counterparts [16, 22]. We expect, as in the case of 3D superfluid turbulence [23–26], that the results from our 2D HVBK studies will be borne out by experiments on 2D superfluid turbulence if these experiments probe length scales that are larger than the mean separation between quantum vortices. To obtain power-law tails in velocity-component PDFs, of the type that have been seen in some experiments in 3D quantum turbulence [27], we must use either (a) the Gross-Pitaevskii (GP) equation [28–30], which can resolve quantum vortices, or (b) Biot-Savart-type models [31]. Two-dimensional superfluid turbulence is now being studied numerically with such models [4, 30, 32, 33]. In particular, some DNS studies have looked for inverse cascades in 2D GP turbulence, which is forced and in which a dissipation term is used to obtain a statistically steady state. One such study [33] has obtained an inverse cascade. On scales that are much larger than the mean separation between quantum vortices, and when quantum vortices of the same sign cluster, we expect superfluids to be described by the HVBK equations, if we restrict ourselves to low-Mach-number flows [4, 9, 10]; and the extraction of HVBK-model parameters from GP studies is just beginning to be studied in 3D [34, 35] and 2D [36, 37].

Our DNS study of homogeneous, isotropic turbulence in the 2D HVBK model has led to the first elucidation of inverse and forward cascades in this system, has contrasted them with their counterparts in 2D fluid turbulence, and led to qualitatively new results that await experimental confirmation in turbulent superfluid films. We have shown that both $E^n(k)$ and $E^s(k)$ exhibit inverse- and forward-cascade power-law regimes. We have demonstrated that, as B increases, $\mathbf{u}_n$ and $\mathbf{u}_s$ tend to align with each other: the PDF $P(\cos(\theta))$ has a peak at $\cos(\theta) = 1$ and $P(\gamma)$ displays power-law tails with universal exponents, which do not depend on B, ρ_n/ρ, and k_f. The parameters B and ρ_n/ρ depend on the temperature; and this dependence has been measured in experiments [38] in 3D; such experimental studies have not been carried out in 2D.

We thank M.E. Brachet and A. Bhatnagar for discussions, CSIR, DST, and UGC (India) for financial support, and SERC (IISc) for computational resources.

* research.vishwanath@gmail.com
† anupam1509@gmail.com
‡ rahul@physics.iisc.ernet.in;
also at Jawaharlal Nehru Centre For Advanced Scientific Research, Jakkur, Bangalore, India.

[1] R. J. Donnelly, *Quantized vortices in helium II* (Cambridge University Press, 1991)

[2] M. S. Paoletti and D. P. Lathrop, Annu. Rev. Condens. Matter Phys. **2**, 213 (2011)
[3] L. Skrbek and K. R. Sreenivasan, Phys. Fluids **24**, 011301 (2012)
[4] N. G. Berloff, M. Brachet, and N. P. Proukakis, Proc. Natl. Acad. Sci. USA **111**, 4675 (2014)
[5] U. Frisch, *Turbulence* (Cambridge University Press, Cambridge, UK, 1996)
[6] M. Lesieur, *Turbulence in fluids* (Kluwer Academic publishers Dordrecht, 1997)
[7] G. Boffetta and R. E. Ecke, Ann. Rev. Fluid Mech. **44**, 427 (2012)
[8] R. Pandit, P. Perlekar, and S. S. Ray, Pramana **73**, 157 (2009)
[9] R. J. Donnelly, J. Phys.: Condensed Matter **11**, 7783 (1999)
[10] C. F. Barenghi, R. J. Donnelly, and W. F. Vinen, J. Low Temp. Phys. **52**, 189 (1983)
[11] H. E. Hall and W. F. Vinen, Proc. Roy. Soc. A **238**, 215 (1956)
[12] I. M. Khalatnikov, *An introduction to the theory of superfluidity* (WA Benjamin New York, 1965)
[13] P. Perlekar and R. Pandit, New J. Phys. **11**, 073003 (2009)
[14] B. Fornberg, *A practical guide to pseudospectral methods* (Cambridge University Press, 1998)
[15] S. M. Cox and P. C. Matthews, J. Comput. Phys. **176**, 430 (Mar. 2002), ISSN 0021-9991
[16] See Supplemental Material for video and additional figures.
[17] P. E. Roche, C. F. Barenghi, and E. Lévêque, Europhys. Lett. **87**, 54006 (2009)
[18] K. Morris, J. Koplik, and D. W. I. Rouson, Phys. Rev. Lett. **101**, 015301 (2008)
[19] D. H. Wacks and C. F. Barenghi, Phys. Rev. B **84**, 184505 (2011)
[20] K. Nam, E. Ott, T. M. Antonsen, and P. N. Guzdar, Phys. Rev. Lett. **84**, 5134 (May 2000)
[21] G. Boffetta, A. Cenedese, S. Espa, and S. Musacchio, Europhys. Lett. **71**, 590 (2005)
[22] A. W. Baggaley and C. F. Barenghi, Phys. Rev. E **84**, 067301 (Dec 2011)
[23] P.-E. Roche, P. Diribarne, T. Didelot, O. Français, L. Rousseau, and H. Willaime, Europhys. Lett. **77**, 66002 (2007)
[24] J. Salort, C. Baudet, B. Castaing, B. Chabaud, F. Daviaud, T. Didelot, P. Diribarne, B. Dubrulle, Y. Gagne, F. Gauthier, *et al.*, Phys. Fluids **22**, 125102 (2010)
[25] J. Salort, B. Chabaud, E. Lévêque, and P.-E. Roche, in *J. Phys. Conf. Ser.*, Vol. 318 (IOP Publishing, 2011) p. 042014
[26] J. Salort, B. Chabaud, E. Lévêque, and P.-E. Roche, Europhys. Lett. **97**, 34006 (2012)
[27] M. S. Paoletti, M. E. Fisher, K. R. Sreenivasan, and D. P. Lathrop, Phys. Rev. Lett. **101**, 154501 (2008)
[28] A. C. White, C. F. Barenghi, N. P. Proukakis, A. J. Youd, and D. H. Wacks, Phys. Rev. Lett. **104**, 075301 (2010)
[29] B. Nowak, J. Schole, D. Sexty, and T. Gasenzer, Phys. Rev. A **85**, 043627 (2012)
[30] V. Shukla, M. Brachet, and R. Pandit, New J. Phys. **15**, 113025 (2013)
[31] H. Adachi and M. Tsubota, Phys. Rev. B **83**, 132503 (2011)
[32] R. Numasato, M. Tsubota, and V. S. L'vov, Phys. Rev. A **81**, 063630 (2010)
[33] M. T. Reeves, T. P. Billam, B. P. Anderson, and A. S. Bradley, Phys. Rev. Lett. **110**, 104501 (2013)
[34] N. G. Berloff and A. J. Youd, Phys. Rev. Lett. **99**, 145301 (Oct 2007)
[35] G. Krstulovic and M. Brachet, Phys. Rev. B **83**, 132506 (Apr 2011)Phys. Rev. E **83**, 066311 (Jun 2011)
[36] B. Jackson, N. P. Proukakis, C. F. Barenghi, and E. Zaremba, Phys. Rev. A **79**, 053615 (May 2009)
[37] V. Shukla, *Particles and Fields in Superfluid Turbulence: Numerical and Theoretical Studies*, Ph.D. thesis, Indian Institute of Science, Bangalore (2014), unpublished
[38] R. J. Donnelly and C. F. Barenghi, J. Phys. Chem. Ref. Data **27**, 1217 (1998)

Supplemental Material

In this Supplemental Material we give details of our calculations; these augment the results that we have presented in the main part of this paper.

Video M1 (`http://youtu.be/-ZDkoxQInXY`)
This video illustrates the spatiotemporal evolution, via pseudocolor plots, of ω_n (left panels) and ω_s (right panels) in which the mutual friction is (a) absent in the top two panels (DNS run `R0`) and (b) present in the lower two panels (DNS run `R1`).

In Table II we give the detailed list of parameters, which we use in our DNS runs. The energy and enstrophy are defined as $E_{\rm i} = \frac{1}{2}\sum_k E_{\rm i}(k)$ and $\Omega_{\rm i} = \frac{1}{2}\sum_k k^2 E_{\rm i}(k)$ ($i \in ({\rm n}, {\rm s})$), respectively. The root-mean-square velocity is $u^{\rm i}_{\rm rms} = \sqrt{E_{\rm i}}$; the Taylor microscale is

$$\ell^{\rm i}_\lambda = \sqrt{\frac{E_{\rm i}}{2\Omega_{\rm i}}}; \tag{5}$$

the Taylor-microscale Reynolds number is

$$Re^{\rm i}_\lambda = \frac{u^{\rm i}_{\rm rms}\ell^{\rm i}_\lambda}{\nu_{\rm i}}; \tag{6}$$

the integral length scale is

$$l^{\rm i}_0 = \frac{\sum_k E_{\rm i}(k)/k}{E_{\rm i}}; \tag{7}$$

the eddy-turnover time is

$$\tau^{\rm i}_{\rm eddy} = \frac{l^{\rm i}_0}{u^{\rm i}_{\rm rms}}; \tag{8}$$

the dissipation scale is

$$\eta_{\rm i} = \Big[\frac{\nu_{\rm i}^2}{2\Omega_{\rm i}}\Big]^{1/4}; \tag{9}$$

here $i \in ({\rm n}, {\rm s})$.

In Fig. 3 we present the pseudocolor plots of ω_n and ω_s for run `R2a` (panels (a) and (b)).

In Fig. 4 we show plots of the cumulative distribution functions (CDFs) $Q(\gamma)$ of $\gamma = |\mathbf{u}_{\rm n}|/|\mathbf{u}_{\rm s}|$, for the runs `R1`, `R2a`-`R2c`, `R5`, and `R6`. These CDFs exhibit power-law tails that imply that the PDF $P(\gamma) \sim \gamma$, for $\gamma \ll 1$; the power-law exponents of these tails of $P(\gamma)$ are universal in the sense that they do not depend on B, $\rho_{\rm n}/\rho$, and $k_{\rm f}$.

In Figs. 5 and 6 we show that the PDFs of the Cartesian components of the normal and superfluid velocities in 2D HVBK turbulence are close to Gaussian (as in 2D, classical-fluid turbulence). Figure 7 shows that the tails of the PDFs of the normal and superfluid vorticity in 2D HVBK turbulence are close to exponentials, as in 2D, classical-fluid turbulence. In Fig. 8 we show the PDFs of the Okubo-Weiss parameter $\Lambda_i = (\omega_i^2 - \sigma_i^2)/4$, $i \in (n, s)$, whose sign determines whether the flow in a given region is vortical ($\Lambda_i > 0$) or strain-dominated ($\Lambda_i < 0$); ω_i^2 and σ_i^2 are the squares of the vorticity and the strain-rate, respectively. These PDFs are similar to their 2D, classical-fluid-turbulence counterparts.

	N_c	ρ_n/ρ	B	ν_n	ν_s	μ_n	μ_s	$k_f^{\rm n}$	$k_f^{\rm s}$	$f_0^{\rm n}$	$f_0^{\rm s}$	$\ell_\lambda^{\rm n}$	$\ell_\lambda^{\rm s}$	Re_λ^n	Re_λ^s	$\tau_{\rm eddy}^{\rm n}$	$\tau_{\rm eddy}^{\rm s}$	$k_{\rm max}\eta_{\rm n}$	$k_{\rm max}\eta_{\rm s}$
R0	1024	–	–	10^{-4}	10^{-5}	10^{-2}	5×10^{-3}	2	2	10^{-3}	10^{-3}	0.36	0.38	92.77	1.25×10^3	51.1	45.8	17.7	5.16
R1	1024	0.1	1.0	10^{-4}	10^{-5}	10^{-2}	5×10^{-3}	2	2	10^{-3}	10^{-3}	0.371	0.378	112.9	1.3×10^3	46.3	42.3	16.8	5.01
R2a	1024	0.1	1.0	10^{-4}	10^{-5}	10^{-2}	5×10^{-3}	–	50	–	10^{-1}	0.062	0.049	108.4	876.7	5.43	5.12	2.89	0.82
R2b	1024	0.1	2.0	10^{-4}	10^{-5}	10^{-2}	5×10^{-3}	–	50	–	10^{-1}	0.058	0.05	100.6	876.8	5.23	5.05	2.80	0.82
R2c	1024	0.1	5.0	10^{-4}	10^{-5}	10^{-2}	5×10^{-3}	–	50	–	10^{-1}	0.054	0.05	94.3	876.5	5.12	5.04	2.7	0.82
R3	1024	0.05	1.0	10^{-4}	10^{-5}	10^{-2}	5×10^{-3}	–	50	–	10^{-1}	0.064	0.051	119.1	976.7	5.03	4.77	2.84	0.771
R4	1024	0.3	1.0	10^{-4}	10^{-5}	10^{-2}	5×10^{-3}	–	50	–	10^{-1}	0.052	0.039	62.9	487.6	5.72	5.14	3.18	0.868
R5	1024	0.5	1.0	10^{-5}	10^{-6}	10^{-2}	5×10^{-3}	–	50	–	10^{-1}	0.043	0.035	484.1	4.1×10^3	4.88	4.49	0.916	0.264
R6	1024	0.9	1.0	10^{-5}	10^{-6}	10^{-2}	5×10^{-3}	50	–	10^{-1}	–	0.039	0.047	617.0	7.19×10^3	3.50	3.84	0.771	0.268

TABLE II. Parameters for our DNS runs R0-R6: ρ_n/ρ is the fraction of the normal fluid, B the mutual-friction coefficient, N_c^2 the number of collocation points, ν_n (ν_s) the normal-fluid (superfluid) kinematic viscosity, μ_n (μ_s) the coefficient of linear friction for the normal fluid (superfluid), and $k_{\rm f}^n$ ($k_{\rm f}^s$) and f_0^n (f_0^s) are the forcing wavevector and the forcing amplitude for the normal fluid (superfluid); ν_s and μ_s should vanish for a superfluid but they are included here for numerical stability, with $\nu_s \ll \nu_n$ and $\mu_s \ll \mu_n$; ℓ_λ^n and ℓ_λ^s are the normal-fluid and superfluid Taylor microscales, Re_λ^n and Re_λ^s the associated Reynolds numbers, $\tau_{\rm eddy}^{\rm n}$ and $\tau_{\rm eddy}^{\rm s}$ the eddy-turnover times; $\eta_{\rm n}$ and $\eta_{\rm s}$ are the dissipation length scales; $k_{\rm max}$ is the magnitude of the largest wave vector in our 2/3-dealiased DNS. In runs R2a-R6 we force the dominant component (i.e., the normal-fluid (superfluid) component if $\rho_n/\rho > 0.5$ ($\rho_n/\rho \leq 0.5$)).

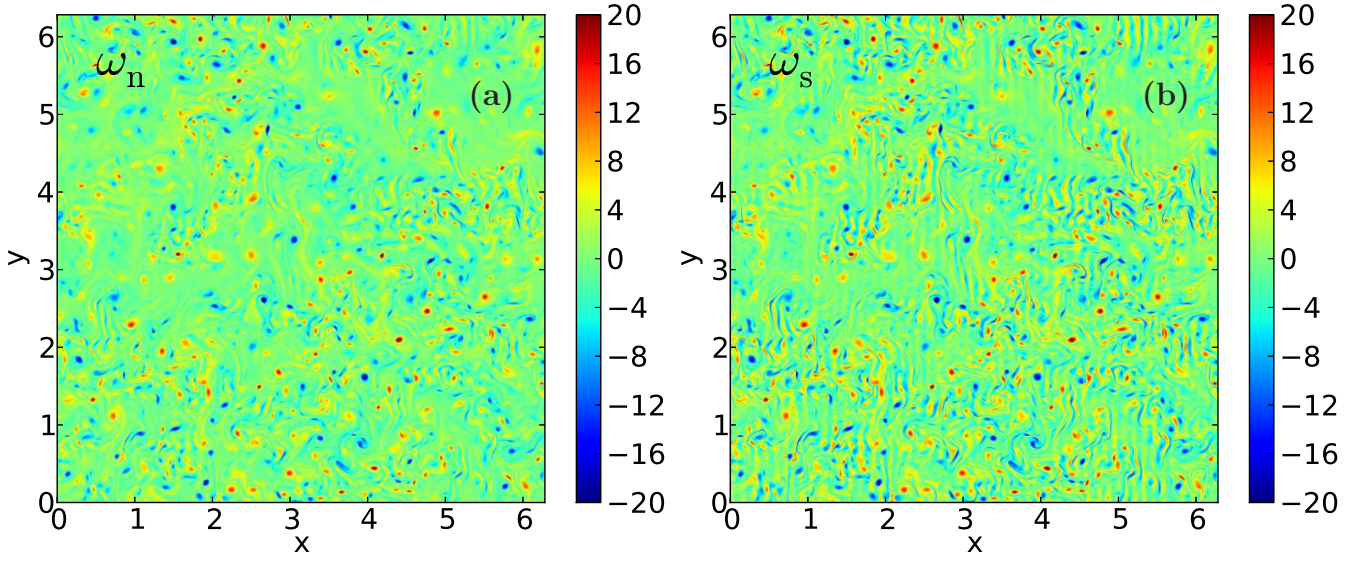

FIG. 3. (Color online) Pseudocolor plots of the vorticity fields, ω_n and ω_s, from our DNS run R2a at $t = 1500$ (panels (c) and (d), $k_{\rm f} = 50$); these plots show that the normal and superfluid component are locked to each other.

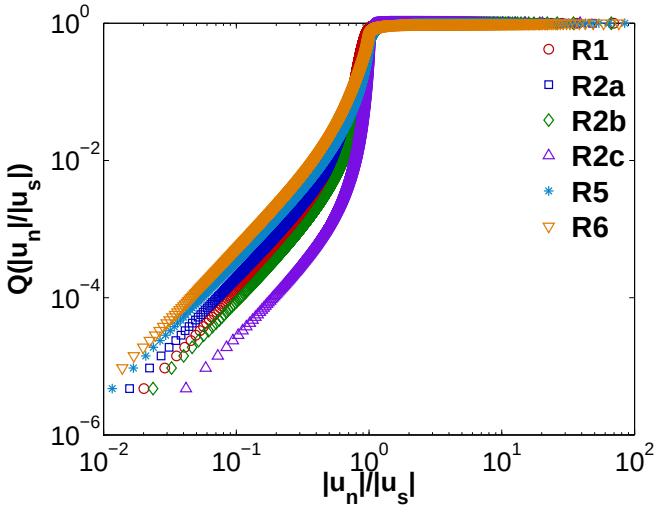

FIG. 4. (Color online) Log-log (base 10) plots of the cumulative distribution functions (CDF) $Q(\gamma)$ of $\gamma = |\mathbf{u}_\mathrm{n}|/|\mathbf{u}_\mathrm{s}|$ for the runs `R1`, `R2a-R2c`, `R5`, and `R6`. These CDFs show power-law tails $Q(\gamma) \sim \gamma^2$, i.e., the PDF $P(\gamma) \sim \gamma$, for $\gamma \ll 1$.

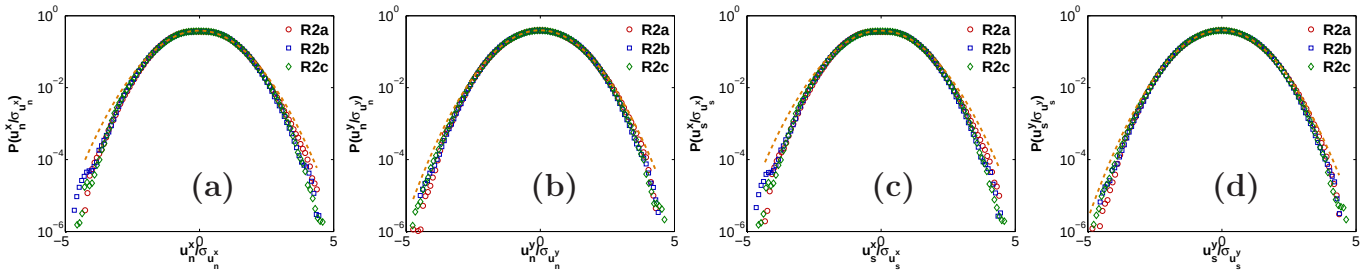

FIG. 5. (Color online) Semilogarithmic (base 10) plots of the PDFs of the (a) x component $\mathbf{u}_\mathrm{n}^x$ and (b) y component $\mathbf{u}_\mathrm{n}^y$ of the normal fluid velocity; PDFs of (c) x component $\mathbf{u}_\mathrm{s}^x$; (d) y component $\mathbf{u}_\mathrm{s}^y$ of the superfluid velocity. $\sigma_{u_\mathrm{i}^\mathrm{j}}$ denotes the standard-deviation of the field u_i^j, here $i \in (\mathrm{n},\mathrm{s})$ and $j \in (\mathrm{x},\mathrm{y})$. These data are from our DNS runs `R2a` (red circles), `R2b` (blue squares), and `R2c` (green diamonds), respectively; the orange dashed line indicates a Gaussian fit.

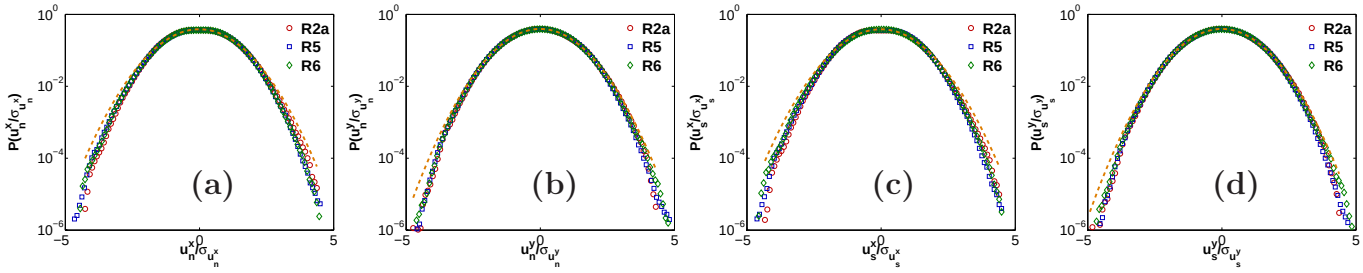

FIG. 6. (Color online) Semilogarithmic (base 10) plots of the PDFs of the (a) x component $\mathbf{u}_\mathrm{n}^x$ and (b) y component $\mathbf{u}_\mathrm{n}^y$ of the normal fluid velocity; PDFs of (c) x component $\mathbf{u}_\mathrm{s}^x$; (d) y component $\mathbf{u}_\mathrm{s}^y$ of the superfluid velocity. $\sigma_{u_\mathrm{i}^\mathrm{j}}$ denotes the standard-deviation of the field u_i^j, here $i \in (\mathrm{n},\mathrm{s})$ and $j \in (\mathrm{x},\mathrm{y})$. These data are from our DNS runs `R2a` (red circles), `R5` (blue squares), and `R6` (green diamonds), respectively; the orange dashed line indicates a Gaussian fit.

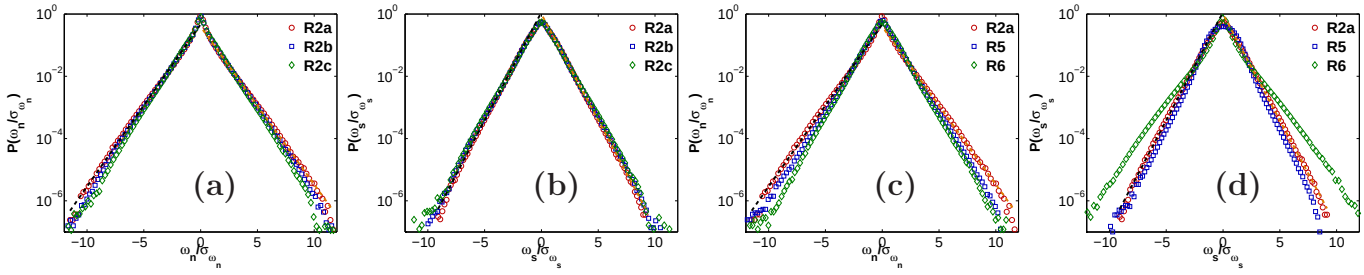

FIG. 7. (Color online) Semilogarithmic (base 10) plots of the PDFs of the vorticity of the (a) normal fluid ($\omega_{\rm n}$) from our DNS runs R2a (red circles), R2b (blue squares), and R2c (green diamonds); the black- and the orange-dashed lines indicate an exponential fit to the left (slope = -0.5064) and the right (slope = 0.5207) branches of the PDF $P(\omega_n/\sigma_{\omega_n})$ for the DNS run R2a; PDFs of the (b) superfluid ($\omega_{\rm s}$) from our DNS runs R2a (red circles), R2b (blue squares), and R2c (green diamonds); the black- and the orange-dashed lines indicate an exponential fit to the left (slope = -0.6818) and the right (slope = 0.6951) branches of the PDF $P(\omega_s/\sigma_{\omega_s})$ for the DNS run R2a; PDFs of the (c) normal fluid ($\omega_{\rm n}$) from our DNS runs R2a (red circles), R5 (blue squares), and R6 (green diamonds); the black- and the orange-dashed lines indicate an exponential fit to the left (slope = -0.5064) and the right (slope = 0.5207) branches of the PDF $P(\omega_n/\sigma_{\omega_n})$ for the DNS run R2a; PDFs of the (d) superfluid ($\omega_{\rm s}$) from our DNS runs R2a (red circles), R5 (blue squares), and R6 (green diamonds); the black- and the orange-dashed lines indicate an exponential fit to the left (slope = -0.6818) and the right (slope = 0.6951) branches of the PDF $P(\omega_s/\sigma_{\omega_s})$ for the DNS run R2a. $\sigma_{\omega_{\rm i}}$ denotes the standard-deviation of the field $\omega_{\rm i}$, here $i \in ({\rm n}, {\rm s})$.

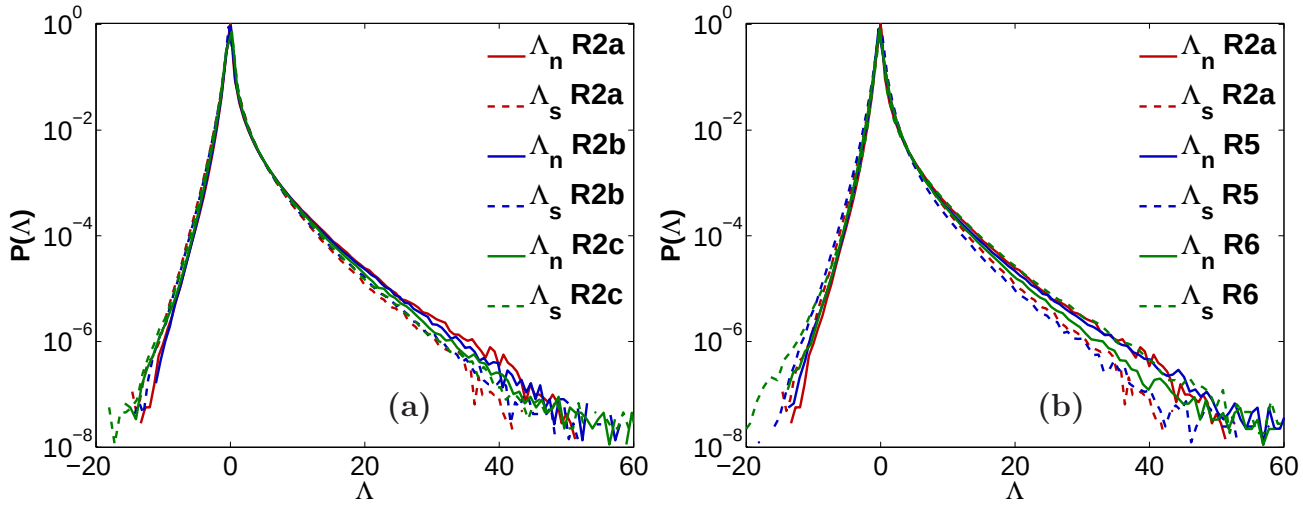

FIG. 8. (Color online) Semilogarthimic (base 10) plots of the PDFs of the Okubo-Weiss parameter for the normal fluid $\Lambda_{\rm n}$ (solid line) and the superfluid $\Lambda_{\rm s}$ (dashed line); (a) R2a (red line), R2b (blue line), and R2c (green line) showing the variation of these PDF with the mutual-friction coefficients $B = 1$, $B = 2$, and $B = 5$, respectively; (b) R2a (red line), R5 (blue line), and R6 (green line) showing the variation of these PDF with the $\rho_{\rm n}/\rho = 0.1$, $\rho_{\rm n}/\rho = 0.5$, and $\rho_{\rm n}/\rho = 0.9$, respectively. In 2D, classical-fluid turbulence, the PDF of the Okubo-Weiss parameter is qualitatively similar [13] to the PDFs shown here.